Published in final edited form as:
*Conf Proc IEEE Eng Med Biol Soc*. 2014 August ; 2014: 1298–1301. doi:10.1109/EMBC.2014.6943836.

# Local field potentials mitigate decline in motor decoding performance caused by loss of spiking units

**Kyle M. Rupp**,
Department of Biomedical Engineering at The Johns Hopkins University, Baltimore, MD, USA

**Marc H. Schieber**, and
Department of Neurology, Neurobiology, and Anatomy, at the University of Rochester Medical Center, Rochester, NY, USA

**Nitish V. Thakor [Fellow, IEEE]**
Department of Biomedical Engineering at The Johns Hopkins University, Baltimore, MD, USA and with the Singapore Institute for Neurotechnology, National University of Singapore, Singapore

Nitish V. Thakor: nitish@jhu.edu

## Abstract

The technology underlying brain computer interfaces has recently undergone rapid development, though a variety of issues remain that are currently preventing it from becoming a viable clinical assistive tool. Though decoding of motor output has been shown to be particularly effective when using spikes, these decoders tend to degrade with the loss of subsets of these signals. One potential solution to this problem is to include features derived from LFP signals in the decoder to mitigate these negative effects. We explored this solution and found that the decline in decoding performance that accompanies spiking unit dropout was significantly reduced when LFP power features were included in the decoder. Additionally, high frequency LFP features in the 100–170 Hz band were more effective than low frequency LFP features in the 2–4 Hz band at protecting the decoder from a dropoff in performance. LFP power appears to be an effective signal to improve the robustness of spiking unit decoders. Future studies will explore online classification and performance improvements in chronic implants by the proposed method.

## I. Introduction

Over the last decade, a preponderance of technological and computational advances have contributed to the growth of the rapidly developing field of brain-computer interfaces, or BCIs. These systems show great promise to restore functions such as limb movement to impaired subjects by transforming recorded neural signals into a desired output and actuating these motor commands via an assistive device. Previous work has already shown that ensembles of spikes (single unit activity, or SUA) are particularly effective at decoding a variety of motor parameters [1]–[5].

While these studies demonstrated impressive results, a number of technological advancements are required to develop a reliable long-term prosthetic device. One particularly difficult challenge relates to establishing stable decoding of neural signals. Decoder instability is closely related to instabilities in the SUA signals; from day to day, the population of available spike signals varies, which can directly result in a degradation in decoding performance [6], [7]. Single units recorded from multielectrode arrays are particularly unstable due to factors that include changes in electrode impedance and micromotion of the electrode arrays [7].

Local field potentials (LFPs) are thought to be composed largely of postsynaptic currents [8], [9] and represent activity from thousands of neurons in the immediate vicinity of the recording microelectrode [10]. Since LFPs represent a large population of neurons relative to spikes, they are believed to be more stable than spikes and may serve as a suitable signal for BCIs [11], [12]. In fact, recent work has shown that movement-related information in LFPs persists even when spikes are lost, indicating that instabilities in SUA do not necessarily lead to a degradation in the information content of LFPs [12]. A number of studies have explored the potential of LFPs for both open-loop [5], [13]–[16] and closed-loop [17] decoding of motor parameters. A subset of these studies have directly compared the performance of LFP decoders to decoders constructed with both SUA [5], [12], [15] and multiunit activity (MUA) [15]–[17]. Although it has consistently been shown that LFPs do not outperform SUA and/or MUA in motor decoding, there is speculation that LFPs could be used to provide robustness to decoders [12]. However, few studies to date have investigated the extent to which LFPs may improve SUA-decoding attempts. One study used LFP to decode movement state while using spike trains to decode kinematics [5], while another study compared an SUA decoder to combined SUA+LFP decoders and found that the combined decoder only performed marginally better [15].

Here we explore the hypothesis that decoders that use both spike counts and LFP power features simultaneously are more impervious to the effects of spiking unit dropout than decoders that use only spikes. A male rhesus macaque was trained to perform a cued center out reach-to-grasp task that included 4 different reach directions and object types. Both spiking units (SU, see Materials and Methods) and LFPs were recorded from putative arm and hand areas of motor cortex and were used to build a number of different decoders to discretely classify the movement type. Specifically, SU, high-and low-frequency LFP features (hfLFP from 100–170 Hz and lfLFP from 2–4 Hz respectively), and combinations of SU and LFP features (SU+hfLFP and SU+lfLFP) were used.

Once the performance of these decoders was characterized, spiking units were virtually dropped from the 3 decoders that included them to observe the detrimental effects of spike dropping on motor decoding. Our results suggest that, with the inclusion of LFP features, decoders are better able to tolerate the loss of a number of spiking units as demonstrated by a reduction in the drop in decoding performance.

# II. Methods

## A. Behavioral task

A male rhesus macaque monkey performed a center out reach-to-grasp task (full details can be found in [18]) in which he was cued to reach from a center "home" handle to one of four radially mounted objects, grasp the object, and manipulate it using his right hand. The objects consisted of a push button, a sphere which could be turned, and two objects which could be pulled toward the subject: a coaxial rod and a perpendicular rod (mallet). Data collected during coaxial rod trials were discarded due to poor grounding that contributed significant noise to the neural recordings. The timecourse of each trial is detailed in Fig. 1.

Objects were cued randomly, with the exception that a failed trial resulted in the same object being cued in the next trial. The session analyzed in this study generated 347 trials.

## B. Neural recordings

Both spike trains and LFPs were recorded using 4 floating microelectrode arrays implanted in contralateral primary motor cortex (see Fig. 2a). Each array had 16 channels to record spikes; 8 of these channels also recorded LFP. A total of 58 spikes and 32 LFP channels were recorded. Spikes were sorted offline using Plexon's spike-sorting software, which yielded a mixture of well-isolated single units as well as multi-units. In this analysis, we were interested in using both signals, which we collectively refer to as spiking units. Local field potentials were hardware bandpass filtered from 0.7–175 Hz and digitized at 1 kHz.

## C. Feature extraction

Firstly, data were aligned to the time of cue presentation. Spectral analysis was performed using a windowing technique known as multi-tapering, which can be found in the Chronux toolbox [19]. Low frequency spectral estimation (<35 Hz) was performed using a 500 ms window to give 2 Hz resolution. Only one taper was used, giving a bandwidth of ±2 Hz. High frequency spectral analysis (>35 Hz) was done with a 250 ms window (4 Hz resolution) and 5 tapers, giving a bandwidth of ±12 Hz. For both low and high frequency analysis, a step size of 5 ms was used.

At a particular time point $t$, a spectrum was generated by analyzing a window of LFP from $t - T$ to $t$, where $T$ represents the window length. The magnitude of the spectra was averaged over the frequency bands of interest, namely 2–4 Hz (lfLFP) and 100–170 Hz (hfLFP). Both of these bands were previously shown to have movement-related variation for this particular monkey and session [18].

## D. Classification

Classification was performed using a Naive Bayes classifier, which estimates the class with highest probability given the input features. In this case, the class corresponds to the object type and the input features correspond to spike counts and/or LFP power. Five-fold cross validation was used, so that the data were split into an 80% training set and a 20% testing set, and the training set was further divided into a 75% model building set and a 25% validation set. Each feature consisted of data within a window of length $w$ that started at

time $t_0$ after cue presentation. Separate models were built for $t_0$ ranging from 0 to 1000 ms at 5 ms intervals and for 0 ms ≤ $w$ ≤1000 − $t_0$ ms. The optimal $t_0$ and $w$ were determined by finding the parameter pair that maximized the average decoding accuracy on the validation set from $t$ = 0 to $t$ = 1000 ms. This optimal model was then evaluated on the testing set. Decoding accuracy was used to evaluate the quality of the decoders and was defined as the fraction of trials that were decoded correctly.

### E. Dropout analysis

To characterize the effect of any number of lost spiking units on a decoder's performance, dropout analysis was performed in the following way. A single spiking unit was dropped at random and the resulting decoding accuracy was calculated. This procedure was repeated 100 times, providing an average estimate of the effect of losing a single spiking unit on the performance of the decoder. Spiking unit dropout was simulated by providing zeros for the spike count for that particular spiking unit. This procedure was then repeated by dropping 2 spiking units at random and so on, providing an estimate on the average effect of spiking unit dropout for any number of spiking units.

Dropout analysis was performed on the SU decoder to characterize the detrimental effects of spiking unit dropout. It was then performed on both the SU+lfLFP and the SU+hfLFP decoders to determine the extent to which each set of LFP features mitigated these detrimental effects.

## III. Results

### A. Classifier performance

Classifiers were separately built and tested for SU, lfLFP, hfLFP, SU+lfLFP, and SU +hfLFP. Spiking units performed better than both the lfLFP and hfLFP features in the classifier (see Fig. 3a). Furthermore, the combined SU+lfLFP and SU+hfLFP classifiers performed similarly to the SU decoder. Interestingly, the timing of the lfLFP decoder's peak appears to coincide with a decline in the hfLFP decoder's performance, suggesting that the two features may complement each other well in a combined LFP decoder. Decoding accuracy rose above the baseline accuracy (defined as the accuracy preceding cue presentation) 110 ms after the cue for both the SU and SU+lfLFP decoders; for the lfLFP, hfLFP, and SU+hfLFP decoders, accuracy exceeded baseline at 460 ms, 200 ms, and 115 ms respectively (single-tailed t-test, Bonferroni-corrected for 201 time points tested, $\alpha$ = $0.05/201 = 2.5 \times 10^{-4}$). In other words, discriminative information was present in the features of the SU, SU+lfLFP, and SU+hfLFP decoders first, followed by the hfLFP decoder, and lastly the lfLFP decoder, as can be seen in Fig. 3a. For comparison, the average reaction time for monkey X is 265 ± 111 ms.

Parameter maps like the one shown in Fig. 3b were used to identify the optimal time window for a particular decoder. The parameters for each decoder are displayed in Fig. 3c. Decoders that incorporated single units (SU, SU+lfLFP, and SU+hfLFP) tended to be optimized when trained on earlier and longer time windows compared to the 2 LFP decoders. Additionally, hfLFP decoders tended to perform best with shorter window lengths than lfLFP decoders.

### B. Dropout analysis

The results of the dropout analysis are displayed in Fig. 4. Decoding performance is shown as a function of number of spiking units dropped and is displayed at both early (450 ms) and late (700 ms) timepoints. These timepoints were selected because they represent the points at which the SU+hfLFP and SU+lfLFP decoders optimally improved upon the SU decoders with regards to spiking unit dropout. Additionally, for each of the 500 iterations of dropout analysis (5 folds of cross validation with 100 iterations each), the difference between the SU +LFP decoders and the SU decoders was summed across all dropped spiking units at each timepoint evaluated. This gave a time-varying estimate for the amount of improvement the decoder experienced from adding each set of LFP features (lf- and hfLFP) in the face of spiking unit dropout. We call this metric the LFP dropout improvement. The average of these 500 estimates is plotted for each timepoint evaluated for both the lfLFP and hfLFP decoders (Fig. 4c). Statistically significant improvement was then determined for both lfLFP and hfLFP features at each timepoint (single-tailed t-test, Bonferroni-corrected for 41 time points tested, $\alpha = 0.05/41 = 1.2 \times 10^{-3}$). Notice that the early and late timepoints chosen for Fig. 4A and 4B represent the timepoints at which the hfLFP and lfLFP dropout improvements were maximized respectively.

These results indicate that decoding performance is negatively affected by spiking unit dropout and that both lfLFP and hfLFP features reduce these negative effects. Interestingly, the addition of hfLFP features to the SU decoder seems to mitigate the effects of spiking unit dropout substantially more than the addition of lfLFP features, in spite of the fact that both feature types contain substantial information about the movement (see Fig. 3).

## IV. Discussion

Our results agree with prior studies showing that the addition of LFP features to a spike train decoder do not improve the performance of the decoder under normal conditions. However, further analysis indicates that these LFP features can offer an advantage over SU-only decoders. Specifically, when a subset of the spiking units are lost and can no longer be recorded, LFP features reduce the extent to which decoding performance declines. The 100–170 Hz frequency band appears to be the most effective, while the 2–4 Hz frequency band offered modest protection against spiking unit dropout.

It is worth noting that the most substantial improvement of SU+hfLFP decoders over SU decoders occurs when many spiking units are dropped. This condition might occur under the case of array micromotion, where all electrodes on a given array shift relative to the neural tissue. Under these circumstances, a number of electrodes may be further from spiking units from which they were recording. In order for the results described here to be valid under these circumstances, it is necessary to assume that the LFP recordings would not change substantially in the case of array micromotion.

Ultimately, LFPs can be recorded from the same arrays as spikes (assuming the appropriate recording hardware is used), and there is negligible computational cost to calculate LFP power features and incorporate them into a decoder. Inclusion of these features, particularly in the 100–170 Hz range, may protect a decoder from substantial declines in decoding

performance caused by spiking unit dropout. For these reasons, it is advantageous to include these features in motor decoding classification schemes.

## Acknowledgments

This work was supported in part by the National Science Foundation under Grant EFRI-1137237 and by the National Institute of Biomedical Imaging and Bioengineering under Grant 5T32EB003383.

## References

1. Wessberg J, Stambaugh CR, Kralik JD, Beck PD, Laubach M, Chapin JK, Kim J, Biggs SJ, Srinivasan MA, Nicolelis MA. Real-time prediction of hand trajectory by ensembles of cortical neurons in primates. Nature. 2000; 408(6810):361–365. [PubMed: 11099043]
2. Taylor DM, Tillery SIH, Schwartz AB. Direct cortical control of 3d neuroprosthetic devices. Science. 2002; 296(5574):1829–1832. [PubMed: 12052948]
3. Velliste M, Perel S, Spalding MC, Whitford AS. A. B. Number of neurons dropped Schwartz, . Cortical control of a prosthetic arm for self-feeding. Nature. 2008; 453(7198):1098–1101. [PubMed: 18509337]
4. Hochberg LR, Bacher D, Jarosiewicz B, Masse NY, Simeral JD, Vogel J, Haddadin S, Liu J, Cash SS, van der Smagt P, et al. Reach and grasp by people with tetraplegia using a neurally controlled robotic arm. Nature. 2012; 485(7398):372–375. [PubMed: 22596161]
5. Aggarwal V, Mollazadeh M, Davidson AG, Schieber MH, Thakor NV. State-based decoding of hand and finger kinematics using neuronal ensemble and lfp activity during dexterous reach-to-grasp movements. Journal of Neurophysiology. 2013; 109(12):3067–3081. [PubMed: 23536714]
6. Ganguly K, Carmena JM. Emergence of a stable cortical map for neuroprosthetic control. PLoS Biology. 2009; 7(7):e1000153. [PubMed: 19621062]
7. Perge JA, Homer ML, Malik WQ, Cash S, Eskandar E, Friehs G, Donoghue JP, Hochberg LR. Intra-day signal instabilities affect decoding performance in an intracortical neural interface system. Journal of Neural Engineering. 2013; 10(3):036004. [PubMed: 23574741]
8. Mitzdorf U. Current source-density method and application in cat cerebral cortex: investigation of evoked potentials and eeg phenomena. Physiological Reviews. 1985; 65(1):37–100. [PubMed: 3880898]
9. Logothetis NK. The underpinnings of the bold functional magnetic resonance imaging signal. The Journal of Neuroscience. 2003; 23(10):3963–3971. [PubMed: 12764080]
10. Rasch MJ, Gretton A, Murayama Y, Maass W, Logothetis NK. Inferring spike trains from local field potentials. Journal of Neurophysiology. 2008; 99(3):1461–1476. [PubMed: 18160425]
11. Andersen RA, Musallam S, Pesaran B. Selecting the signals for a brain–machine interface. Current Opinion in Neurobiology. 2004; 14(6):720–726. [PubMed: 15582374]
12. Flint RD, Lindberg EW, Jordan LR, Miller LE, Slutzky MW. Accurate decoding of reaching movements from field potentials in the absence of spikes. Journal of Neural Engineering. 2012; 9(4):046006. [PubMed: 22733013]
13. Rickert J, de Oliveira SC, Vaadia E, Aertsen A, Rotter S, Mehring C. Encoding of movement direction in different frequency ranges of motor cortical local field potentials. The Journal of Neuroscience. 2005; 25(39):8815–8824. [PubMed: 16192371]
14. Zhuang J, Truccolo W, Vargas-Irwin C, Donoghue JP. Decoding 3-d reach and grasp kinematics from high-frequency local field potentials in primate primary motor cortex. IEEE Trans Biomed Eng. 2010; 57(7):1774–1784. [PubMed: 20403782]
15. Bansal AK, Truccolo W, Vargas-Irwin CE, Donoghue JP. Decoding 3d reach and grasp from hybrid signals in motor and premotor cortices: spikes, multiunit activity, and local field potentials. Journal of Neurophysiology. 2012; 107(5):1337–1355. [PubMed: 22157115]
16. Stark E, Abeles M. Predicting movement from multiunit activity. The Journal of Neuroscience. 2007; 27(31):8387–8394. [PubMed: 17670985]

17. Flint RD, Wright ZA, Scheid MR, Slutzky MW. Long term, stable brain machine interface performance using local field potentials and multiunit spikes. Journal of Neural Engineering. 2013; 10(5):056005. [PubMed: 23918061]

18. Mollazadeh M, Aggarwal V, Davidson AG, Law AJ, Thakor NV, Schieber MH. Spatiotemporal variation of multiple neurophysiological signals in the primary motor cortex during dexterous reach-to-grasp movements. The Journal of Neuroscience. 2011; 31(43):15 531–15 543. [PubMed: 21209185]

19. Bokil H, Andrews P, Kulkarni JE, Mehta S, Mitra PP. Chronux: a platform for analyzing neural signals. Journal of Neuroscience Methods. 2010; 192(1):146–151. [PubMed: 20637804]

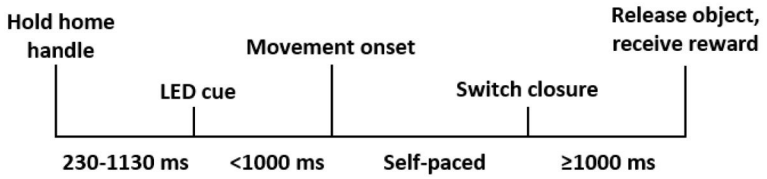


**Fig. 1.**

Each successful task conforms to the shown timeline. From movement onset, the monkey has 10 s to reach to the correct object and close the switch before the trial is aborted and labeled a failure.

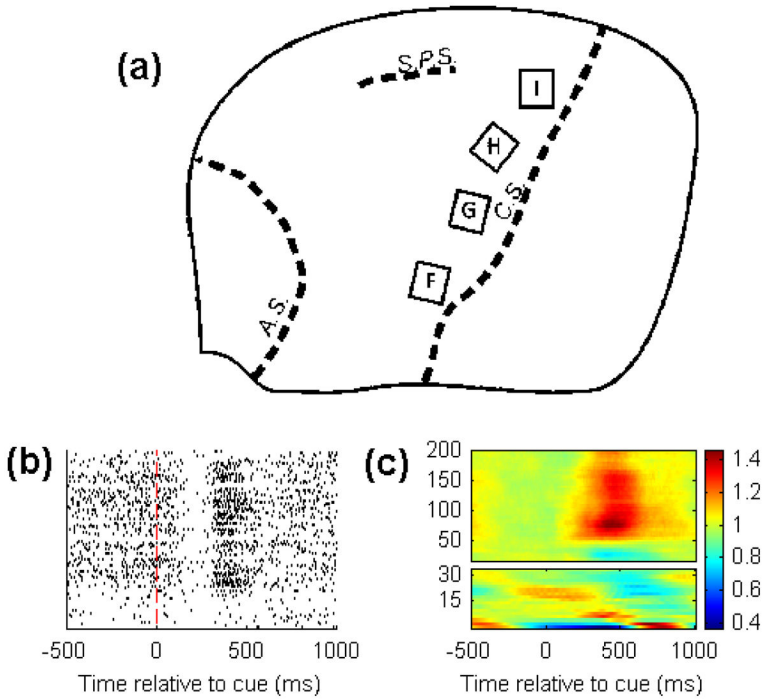


**Fig. 2.**

(a) Arrays F, G, H, and I were implanted anterior to the central sulcus in the putative arm and hand area of M1. (b) A raster plot of a characteristic spike for all sphere trials. (c) The average relative power spectrogram for all successful sphere trials taken from the same electrode. The relative power spectrogram was calculated by dividing the power at each frequency and timepoint by the baseline power at each frequency, where baseline power was defined as the average power from −500 ms to 0 ms for all trials of a particular type.

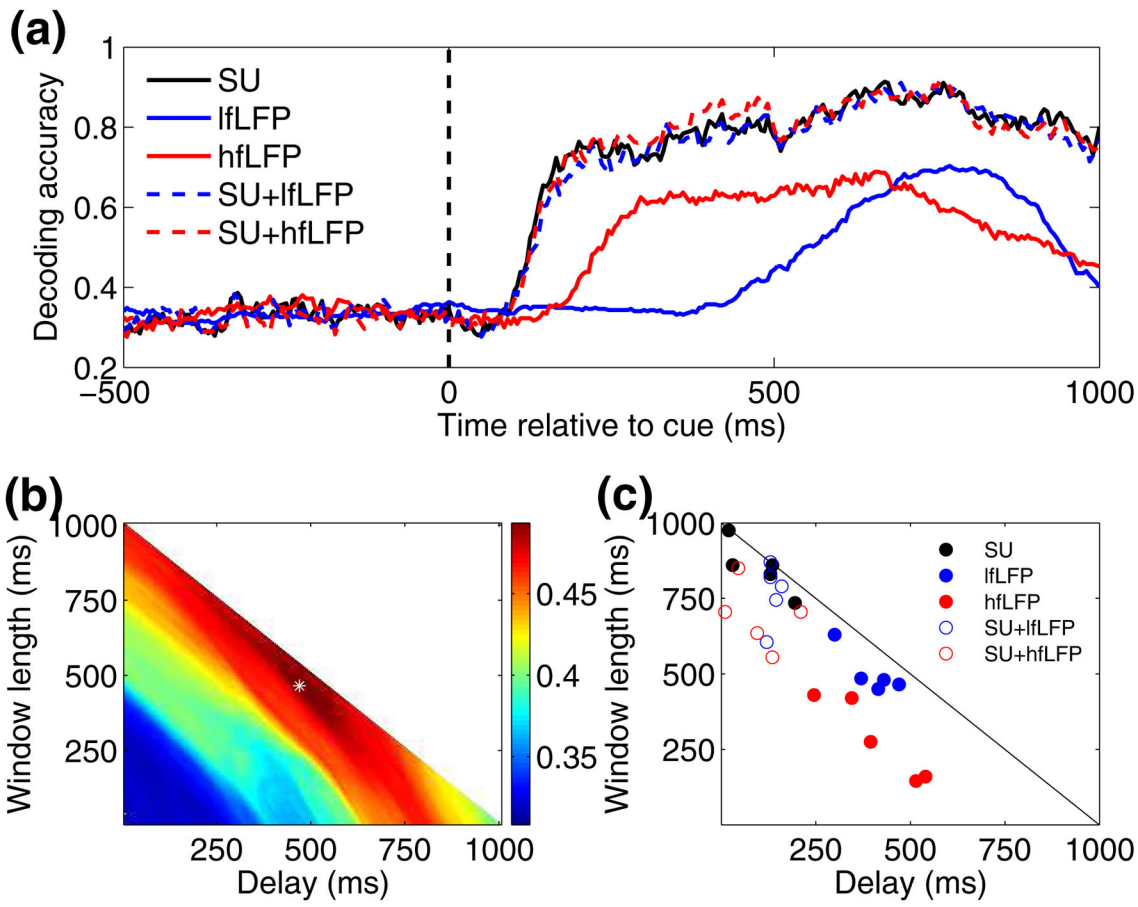


**Fig. 3.**

(a) Decoding accuracy over time is plotted between 3 distinct reach and grasp movements for each of the decoders constructed. Each line represents an average over the 5 cross-validation folds. (b) An example of a parameter map to identify the optimal delay ($t_0$) and time window ($w$) parameters for the lfLFP decoder, where color represents the average decoding accuracy over the 1000 ms window following cue presentation. The white asterisk represents the ($t_0$, $w$) pair that maximizes decoding accuracy in the validation set and was thus chosen for this particular lfLFP decoder. (c) All ($t_0$, $w$) parameter pairs chosen for each decoder. Five points per decoder correspond to each of the decoders constructed using 5-fold cross validation.

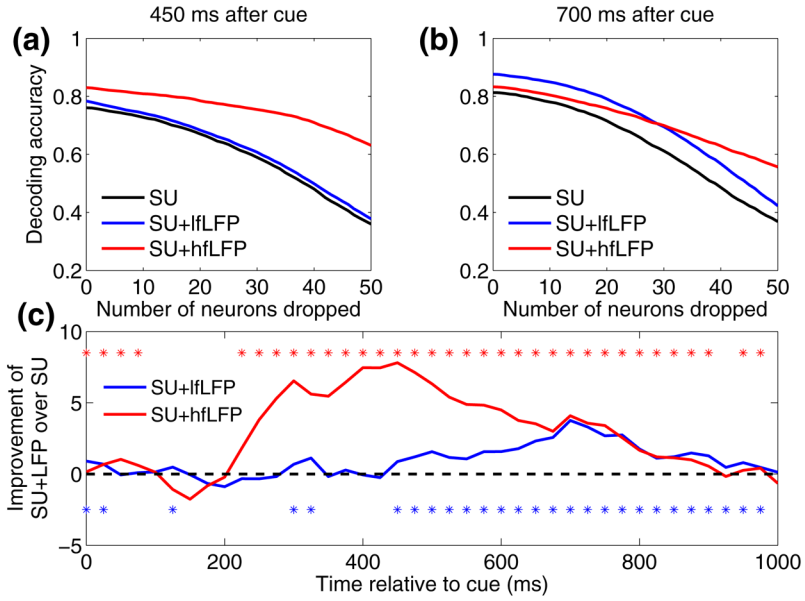


**Fig. 4.**

The average decoding performance versus number of neurons dropped is shown at (a) 450 ms and (b) 700 ms after cue presentation. These results are averaged over 100 repetitions of the dropout analysis for each of the 5 folds of cross-validation. (c) The difference between the SU+LFP and SU decoders at each timepoint evaluated was averaged and plotted here. Asterisks show the timepoints where these differences are statistically larger than zero, indicating that the LFP features improved the decoder under the spiking unit dropout conditions.